LAWRENCE
LIVERMORE
NATIONAL
LABORATORY

UCRL-CONF-216120

Density and Temperature Profile Modifications with Electron Cyclotron Power Injection in Quiescent Double Barrier Discharges on DIII-D

T. A. Casper, K. H. Burrell, E. J. Doyle, P. Gohil, C. J. Lasnier, A. W. Leonard, J. M. Moller, T. H. Osborne, P. B. Snyder, D. M. Thomas, J. Weiland, W. P. West

October 12, 2005

International Atomic Energy Agency H Mode Workshop
St. Petersburg, Russia
September 28, 2005 through September 30, 2005

Density and temperature profile modifications with electron cyclotron power injection in quiescent double barrier discharges on DIII-D

T.A. Casper[a)], K.H. Burrell[b)], E.J. Doyle[c)], P. Gohil[b)], C.J. Lasnier[a)], A.W. Leonard[b)], J.M. Moller[a)], T.H. Osborne[b)], P.B. Snyder[b)], D.M. Thomas[b)], J. Weiland[d)], and W.P. West[b)]

[a)]*Lawrence Livermore National Laboratory, Livermore, California*

[b)]*General Atomics, San Diego, California 92186-5608*

[c)]*University of California, Los Angeles, California 98009*

[d)]*Chalmers University of Technology & EURATOM-VR Association, Gothenburg, Sweden*

Abstract. Quiescent double barrier (QDB) conditions often form when an internal transport barrier is created with high-power neutral-beam injection into a quiescent H-mode (QH) plasma. These QH-modes offer an attractive, high-performance operating scenario for burning plasma experiments due to their quasi-stationarity and lack of edge localized modes (ELMs). Our initial experiments and modeling using ECH/ECCD in QDB shots were designed to control the current profile and, indeed, we have observed a strong dependence on the q-profile when EC-power is used inside the core transport barrier region. While strong electron heating is observed with EC power injection, we also observe a drop in the other core parameters; ion temperature and rotation, electron density and impurity concentration. These dynamically changing conditions provide a rapid evolution of T_e T_i profiles accessible with $0.3 < (T_e\ T_i)_{axis} < 0.8$ observed in QDB discharges. We are exploring the correlation and effects of observed density profile changes with respect to these time-dependent variations in the temperature ratio. Thermal

and particle diffusivity calculations over this temperature ratio range indicate a consistency between the rise in temperature ratio and an increase in transport corresponding to the observed change in density.

I. Introduction

High confinement mode (H-mode) operation is a leading scenario for burning plasma devices [1,2] due to its inherently high energy-confinement characteristics. The quiescent H-mode (QH-mode) [3,4] potentially offers these same advantages with the additional attraction of more steady edge conditions where the highly transient power loads due to edge localized mode (ELM) activity is replaced by the steadier power and particle losses associated with an edge harmonic oscillation (EHO) [3-5]. With the addition of an internal transport barrier (ITB), the capability is introduced for independent control of both the edge conditions and the core confinement region giving possible control of fusion power production in this advanced-tokamak (AT) configuration. The quiescent double barrier (QDB) [3-9] conditions explored in DIII-D experiments exhibit these characteristics and have resulted in steady plasma conditions for several energy confinement times.

To date, we require particle control using divertor cryopumping along with neutral-beam injection opposite to the plasma current [counter-neutral beam injection (NBI)] to achieve QDB-mode operation in DIII-D. We are able to achieve QDB-mode conditions over a fairly wide range of operating conditions [10] including pedestal stored energy and collisionality consistent with ITER operational needs. We observe this operation to be extremely robust and maintain the QH-mode edge conditions where the pedestal region remains edge localized mode (ELM)-free with particle exhaust due to the presence of the EHO. We have found that edge stability is consistent with a model based on peeling-ballooning-mode theory [11]. Recent experiments have explored techniques to expand the operating parameters and to control the pressure and current density profiles. As indicated in figure 1, ramping the triangularity, δ, [10,12] increases the operating density consistent with the predicted effects of strong shaping on stability. Electron cyclotron

heating (ECH) and current drive (ECCD) have resulted in modification of the current and q profiles consistent with modeling predictions [6,8,9]. In both these triangularity ramping and ECCD experiments, we have observed a modification density and temperature profiles.

In the EC injection experiments, figure 2, along with the electron heating we also observed a reduction in density peaking, impurity content and ion temperature similar to that observed in other experiments [13]. In recent experiments to enhance the QDB parameter range [10,12], we used this effect of EC power to control the density profile while ramping the neutral beam power injection to achieve the $\beta_N \sim 3$ shown in figure 1.

II. Internal transport barrier (ITB) in QDB operation

Typically, QH-mode discharges exhibit a propensity for forming a core transport barrier that, in addition to the edge barrier, results in the QDB conditions. With the enhanced core confinement due to formation of the transport barrier, injection of additional NBI power and its fueling in the core can result in pressure profile peaking and β limits. However, these QDB-mode plasmas remain markedly resilient to changes in auxiliary heating power [10] where up to 3 MW of EC power plus 15 MW of NBI have been injected without loss of the desirable, ELM-free pedestal conditions. We find that, once a threshold in injected power is reached, the edge pedestal conditions remain constant while the core conditions can rise dramatically with the formation of a core transport barrier as indicated by the ion temperature and density profiles shown in figure 3. This saturation in edge conditions, while not currently fully understood, results in the resilience of QDB discharges to changes in the injected power. Corsica [14] transport analysis results shown in figure 3 indicate that ion thermal confinement inside the ITB ($\rho \lesssim 0.6$) continues to improve with increased NBI power where χ_i continues to decrease at the higher powers. This indicates that the core ion thermal transport barrier continues to strengthen with χ_i approaching neoclassical, χ_i^{neo}, levels. The core particle diffusivity, however, remains relatively constant inside the ITB with changing NBI power indicating that the density peaking is a more a result of good particle confinement of the beam-injected ions deposited in the core.

III. EC power affects on density profiles

To evaluate the effects of injecting EC power on confinement, we use a discharge representative of our standard, "simple" QDB conditions, namely constant NBI power and no triangularity ramp. Ramping of either NBI power or triangularity also result in changes to the density and temperature profiles that compete with the effects of EC power injection. For our transport analysis, we use shot 110874 shown in figure 2. The effects of EC power on the various profiles is rather dramatic on this shot (but typical of other shots in these experiments) where T_e is observed to rise due to intense electron heating while n_e and T_i drop precipitously during the EC pulse. For this shot, 2 MW of EC power is being injected in the counter-ECCD direction (data from a current profile modification experiment) at $\rho = 0.3$ localized over $\delta\rho = \pm 0.1$ as determined from TORAY-GA [8,15] ray tracing calculations. In several experiments [8,9], we have observed that the effects of EC power on these profiles is not strongly dependent on the antenna aiming, co-ECCD, radial, and counter-ECCD all resulting in similar changes to the profiles.

Using Corsica, we evaluated the change in transport characteristics resulting during injection of EC power. We show results of this analysis in figure 4 at 2.5 s just prior to initiation of ECH, at 2.55 s during the rapid change in confinement, at 2.58 s, 2.61 s and 2.9 s during the more steady conditions with ECH on, and at 4 s after ECH has been turned off and the plasma has returned to a state similar to that before ECH/ECCD. In figure 4 we show spline fits to the measured ion temperature profile (from the CER diagnostic) and the inferred ion density determined by quasi-neutrality from fitting the measured electron (Thomson scattering) and impurity densities (from CER). The corresponding ion thermal, χ_i, and particle, D_i, diffusivities shown in figure 4 indicate the dramatic change in transport resulting from injecting EC power inside the ITB where

χ_i and D_i vary by a factor of 10 inside the barrier region, e.g. $\rho < 0.5$. Analysis at $\rho > 0.85$ has high uncertainty due to poor information on particle fueling and wall recycling.

IV. Consistency with stability models

During the evolution with ECH on, as indicated in figure 2, there is a rapid variation of the electron (T_e) and ion (T_i) temperature profiles with T_e rising due to strong electron heating and T_i falling due to the change in transport characteristics inside the barrier region. This effectively scans the temperature ratio profile, $T_{ei}(\rho) = T_e(\rho)/T_i(\rho)$, figure 5, in the core over the range of on-axis values $0.35 < T_{ei}(0) < 0.75$. Over this range, there is expected to be a large variation in the stability to ion temperature gradient (ITG) and/or trapped electron (TE) modes. To estimate this effect, we compare the temperature scale lengths to the local stability thresholds given by Weiland [16] where the local ITG threshold is

$$\frac{R}{L_{Ti}} = \frac{4}{3\varepsilon_n} + \frac{20}{9T_{ei}}\frac{1}{1+\Gamma} - \frac{T_{ei}}{\varepsilon_n}(1+\Gamma) + \frac{T_{ei}}{2}(1+\Gamma) + \frac{T_{ei}}{2\varepsilon_n^2}(1+\Gamma) \quad ,$$

with $\Gamma = f_T/f_P$ (ratio of trapped to passing particles), ε_n the ratio of electron density to magnetic field scale lengths and L_{Ti} the ion temperature gradient scale lengths. The TE threshold, independent of T_{ei}, is given by

$$\frac{R}{L_{Te}} = \frac{4}{3\varepsilon_n} + \frac{20}{9\Gamma} + \frac{\Gamma}{2}\left(1 - \frac{1}{\varepsilon_n}\right)^2 \quad ,$$

where L_{Te} is the and electron temperature gradient scale length.

In figure 6, we plot time-averaged local ITG threshold profiles and the ion-temperature-gradient scale lengths before, during, and after ECH is applied on shot 110874. Before the onset of ECH (and also after its termination, not shown), the core ($\rho < 0.5$) R/L_{Ti} is significantly less that the local stability threshold, consistent with the fact that core $\chi_i \sim \chi_e^{neo}$. However, during the ECH pulse, the threshold for onset of the ITG mode is comparable to that of the R/L_{Ti} which often exceeds this threshold

condition, an indication that the ITG mode is a likely candidate for driving the enhanced transport during the ECH pulse resulting in the profile modification. In particular, as shown in figure 6, immediately after the ECH is terminated, the plasma rapidly evolves back to the peaked n_e and T_i profiles indicated by the rise in parameters in figure 2 after 3.5 s and the profiles in figure 4 and low $T_{ei}(0)$ in figure 5 both shown at $t = 4$ s. The time variations of the R/L_{Ti}-profiles shown in figure 6 indicate evolution of R/L_{Ti} from significantly higher than the (average) threshold to well below the threshold after a few hundred milliseconds as the plasma reverts back to the strong barrier conditions. This is dominated by the evolution of the ITG threshold over time as indicated in figure 7. In figure 8, we also show the average TE threshold and the electron temperature gradient scale length during the ECH pulse. The plot of R/L_{Te} shown is the closest it gets to the TE threshold indicating that it may be an issue during strong ECH. However, over most of the plasma evolution for this QDB discharge, L_{Te} remains significantly less than the TE-mode threshold indicating that the trapped electron mode is not a likely candidate for causing enhanced transport. Well before and after the ECH and even during the rapid profile evolution at onset and termination of ECH, the R/L_{Te} remains significantly far from this threshold. To better identify and quantify the root cause of transport, additional calculations using codes such as GYRO or GS2 may be required but this is beyond the scope of this paper.

V. Summary.

Quiescent double barrier discharges represent a potentially attractive mode of operation for burning plasmas due to their high β, quiescent edge conditions and potential for discharge control. Additional neutral-beam heating increases the strength of the ion thermal transport barrier with peaking of the density resulting from the low particle transport and the good confinement of ions born in the core region. Injecting EC power into the internal barrier region has been shown to affect the ion confinement properties and the density and temperature profiles. Both the ion thermal and particle diffusivities rise considerably during the EC pulse. This change in confinement correlates with a rise in the electron-to-ion temperature ratio during ECH resulting from both increased electron heating raising T_e and changing transport reducing T_i, consistent with modification of the ITG stability thresholds. This change in transport has been used to advantage for controlling the pressure peaking while increasing the neutral-beam heating to raise the stored energy and obtain $\beta_N \sim 3$ in recent experiments.

Acknowledgment

This work was supported by the U.S. Department of Energy by UC, LLNL under contract W-7405-Eng-48, along with DE-AC02-04ER54698, and DE-FG03-01ER54615.

References

[1] ITER Physics Basis Document, Nucl. Fusion **39**, 2137 (1999).

[2] T.S. Taylor, Plasma Phys. Control. Fusion **39**, B47 (1997).

[3] K.H. Burrell, et al., Phys. Plasmas **82**, 153 (2001).

[4] E.J. Doyle, et al., Plasma Phys. and Control. Fusion **43**, A95 (2001).

[5] C.M. Greenfield, et al., Phys. Rev. Lett. **20**, 4544 (2001).

[6] T.A. Casper, et al., "Current Drive and Pressure Profile Modification with Electron Cyclotron Power in DIII-D Quiescent Double Barrier Experiments," Proceedings of 30th European Conference on Controlled Fusion and Plasma Physics, St. Petersburg, Russia, 2003 (European Physical Society, 2003).

[7] C.M. Greenfield, et al., Plasma Phys and Control. Fusion **44**, A123 (2002).

[8] T.A. Casper, et al., "DIII-D Quiescent Double Barrier Regime Experiments and Modeling," Proceedings of 29th European Conference on Controlled Fusion and Plasma Physics, Montreux, Switzerland, 2002.

[9] E.J. Doyle, et al., "Core and Edge Aspects of Quiescent Double Barrier Operation on DIII-D With Relevance to Critical ITB Physics Issues," Proceedings of 19th IAEA Fusion Energy Conference, Lyon, France, 2002 (International Atomic Energy Agency, Vienna) Paper EX/C3-2.

[10] K.H. Burrell, et al., Phys. Plasmas **12**, 05121 (2005).

[11] P.B. Snyder, et al., "Progress in the Peeling-Ballooning Model of ELMs Toroidal Rotation and 3D Nonlinear Dynamics," Proceedings of 31st European Conference on Plasma Physics, London, United Kingdom, 2004, ECA Vol. 28G (European Physical Society, 2004) P-2.156.

[12] T.A. Casper, et al., "Operational Enhancements in DIII-D Quiescent H-Mode Plasmas," Proceedings of 32nd European Conference on Plasma Physics, Tarragona, Spain, 2005, (European Physical Society, 2005).

[13] A.C.C. Sips, *et al*., Plasma Phys. Control. Fusion **44**, B69 (2002).

[14] J.A. Crotinger, et al., Lawrence Livermore National Report UCRL-ID-126284, 1997 available through NTIS #PB2005-102154.

[15] Y.R. Lin-Liu, et al., Radio Frequency Power in Plasmas: Proceedings of the 12th Topical Conference CP403 (195) 1997.

[16] J. Weiland, et al., "Effects of Temperature Ratio on JET Transport in Hot Ion and Hot Electron Regimes," Proceedings of 31st European Conference on Plasma Physics, London, United Kingdom, 2004, ECA Vol. 28G (European Physical Society, 2004) P-1.160.

List of Figure Captions

Fig 1. Shot 118838: NBI power ramp while using EC power to control the density rise and obtain $\beta_N \sim 3$ and maintain $q_{min} \sim 1.5$ in QDB-mode. δ-ramp for higher density operation is also present. Shot 118821 is a QDB reference shot.

Fig. 2. Shot 110874 typical of changes in parameters induced by ECH power injection; 110850 is a no-ECH reference. I_{imp} is the impurity photon emission rate.

Fig. 3. Profiles of electron density and particle diffusivity and ion temperature and thermal diffusivity during the NBI power scan indicating ITB characteristics of QDB.

Fig. 4. Ion temperature and density and the resulting thermal diffusivity, χ_i, and particle diffusion, D_i, for 110874 indicating change in core transport during ECH.

Fig. 5. T_e/T_i ratio during ECH suggesting changes in ITG stability.

Fig. 6. Time-average ITG thresholds and variations in R/L_{Ti} before, during and after ECH. Before ECH, R/L_{Ti} is well below the threshold. During transition in profiles shortly after ECH is terminated, R/L_{Ti} exceeds the threshold while it is close to the threshold during the steady ECH conditions.

Fig 7. Changes in the ITG threshold dominate ECH evolution.

Fig. 8. Time-average TE threshold and R/L_{Te} during ECH pulse. Over most of this discharge, electron gradient scale length remains far from the threshold.

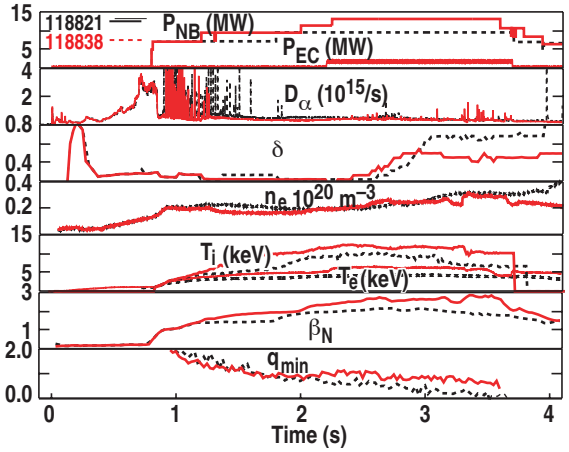
118821
118838
P_{NB} (MW)
P_{EC} (MW)
D_α (10^{15}/s)
δ
n_e 10^{20} m^{-3}
T_i (keV)
T_e (keV)
β_N
q_{min}
Time (s)

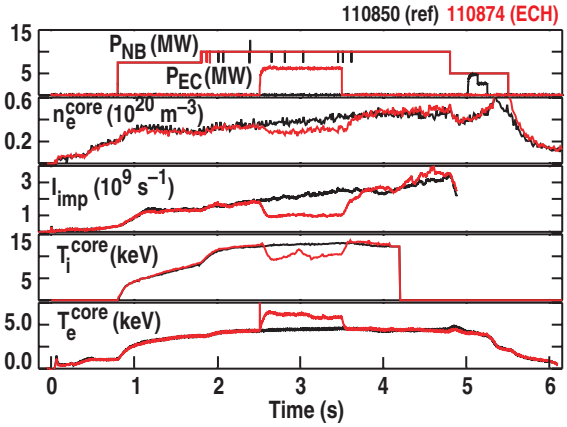
110850 (ref) 110874 (ECH)
15
5
P_{NB} (MW)
P_{EC} (MW)
0.6
0.2
n_e^{core} (10^{20} m^{-3})
3
1
I_{imp} (10^9 s^{-1})
15
5
T_i^{core} (keV)
5.0
0.0
T_e^{core} (keV)
0
1
2
3
4
5
6
Time (s)

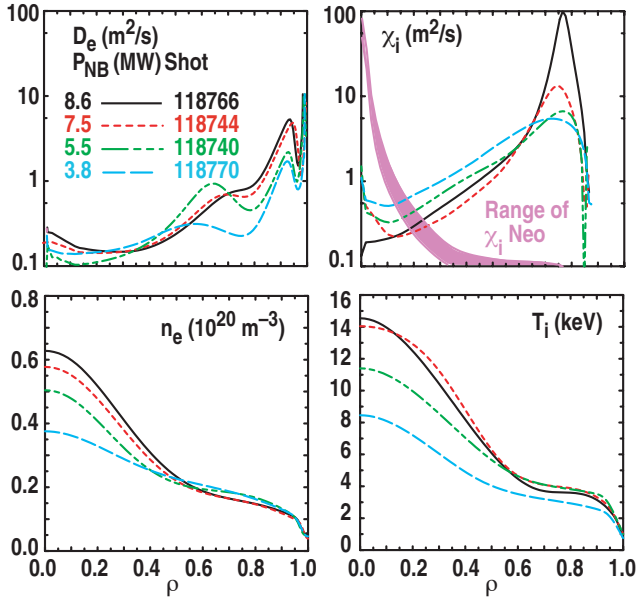
D_e (m^2/s)
P_{NB} (MW) Shot
8.6 118766
7.5 118744
5.5 118740
3.8 118770
χ_i (m^2/s)
Range of χ_i Neo
n_e (10^{20} m^{-3})
T_i (keV)
ρ
ρ

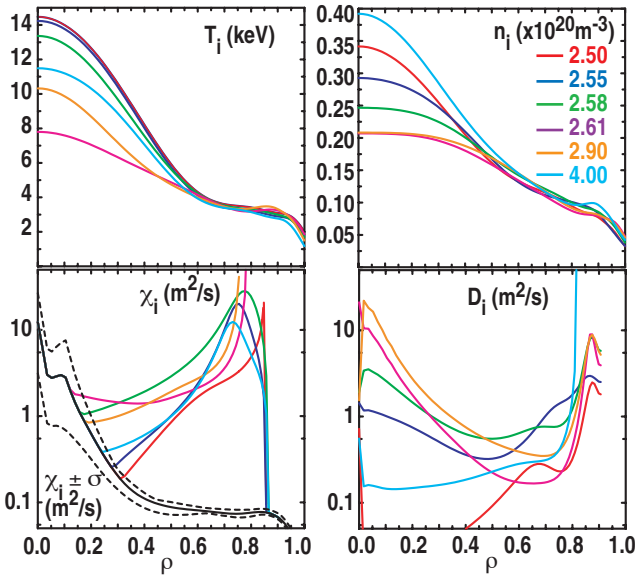
T_i (keV)
n_i (x10^20m^-3)
2.50
2.55
2.58
2.61
2.90
4.00
χ_i (m^2/s)
χ_i ± σ (m^2/s)
D_i (m^2/s)
ρ
ρ

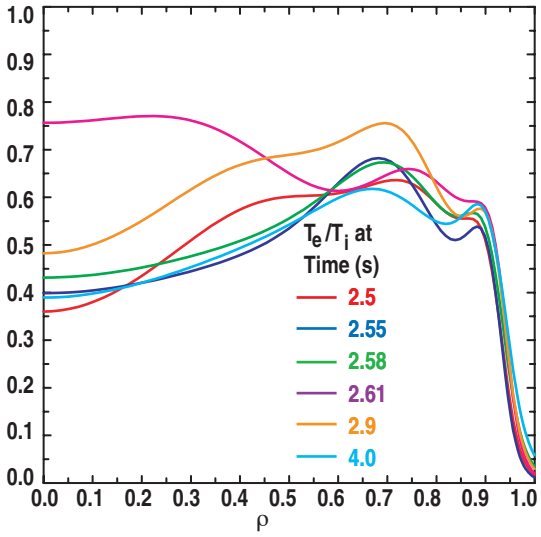
1.0
0.9
0.8
0.7
0.6
0.5
0.4
0.3
0.2
0.1
0.0
0.0 0.1 0.2 0.3 0.4 0.5 0.6 0.7 0.8 0.9 1.0
ρ
Te/Ti at
Time (s)
2.5
2.55
2.58
2.61
2.9
4.0

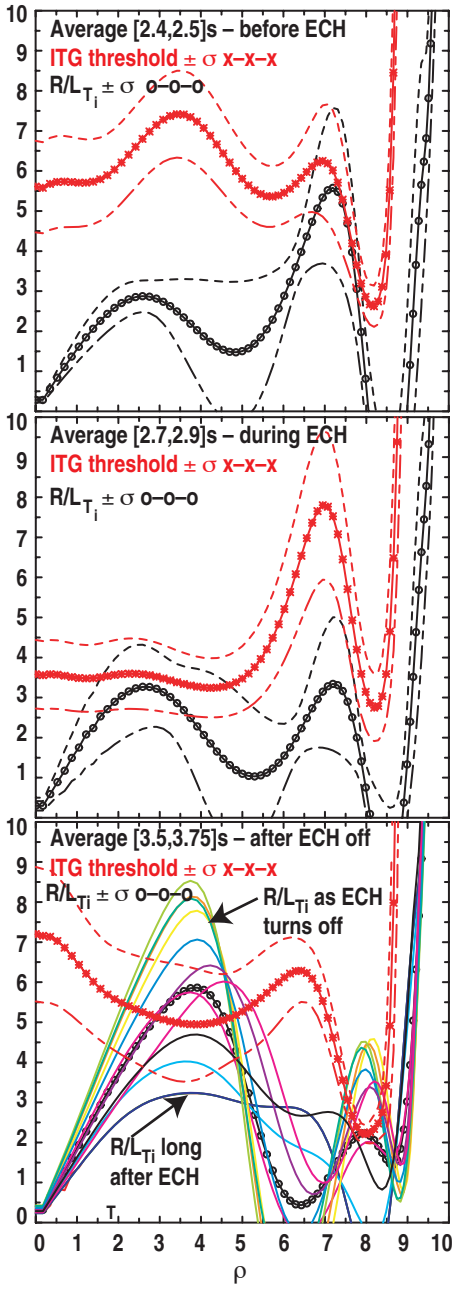
Average [2.4,2.5]s – before ECH
ITG threshold ± σ x–x–x
R/L$_{T_i}$ ± σ o–o–o
Average [2.7,2.9]s – during ECH
ITG threshold ± σ x–x–x
R/L$_{T_i}$ ± σ o–o–o
Average [3.5,3.75]s – after ECH off
ITG threshold ± σ x–x–x
R/L$_{Ti}$ ± σ o–o–o
R/L$_{Ti}$ as ECH turns off
R/L$_{Ti}$ long after ECH
T_i
ρ

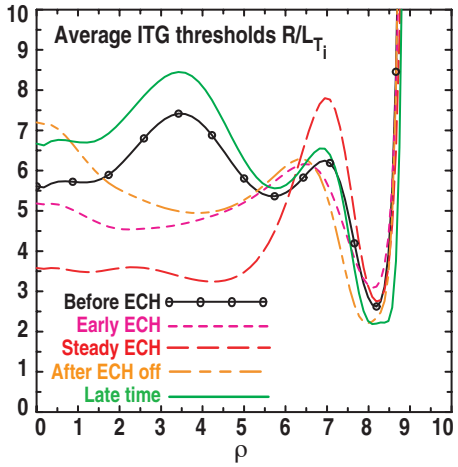
Average ITG thresholds R/L$_{T_i}$
Before ECH
Early ECH
Steady ECH
After ECH off
Late time
ρ

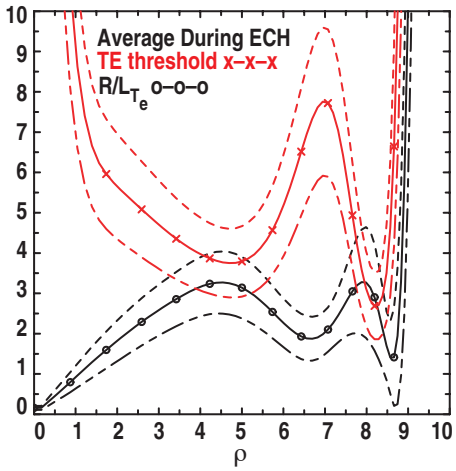
Average During ECH
TE threshold x–x–x
R/L$_{T_e}$ o–o–o
0
1
2
3
4
5
6
7
8
9
10
ρ